Volume 54
Number 47
21 December 2025
Pages 17349-17676

Dalton Transactions

An international journal of inorganic chemistry

rsc.li/dalton

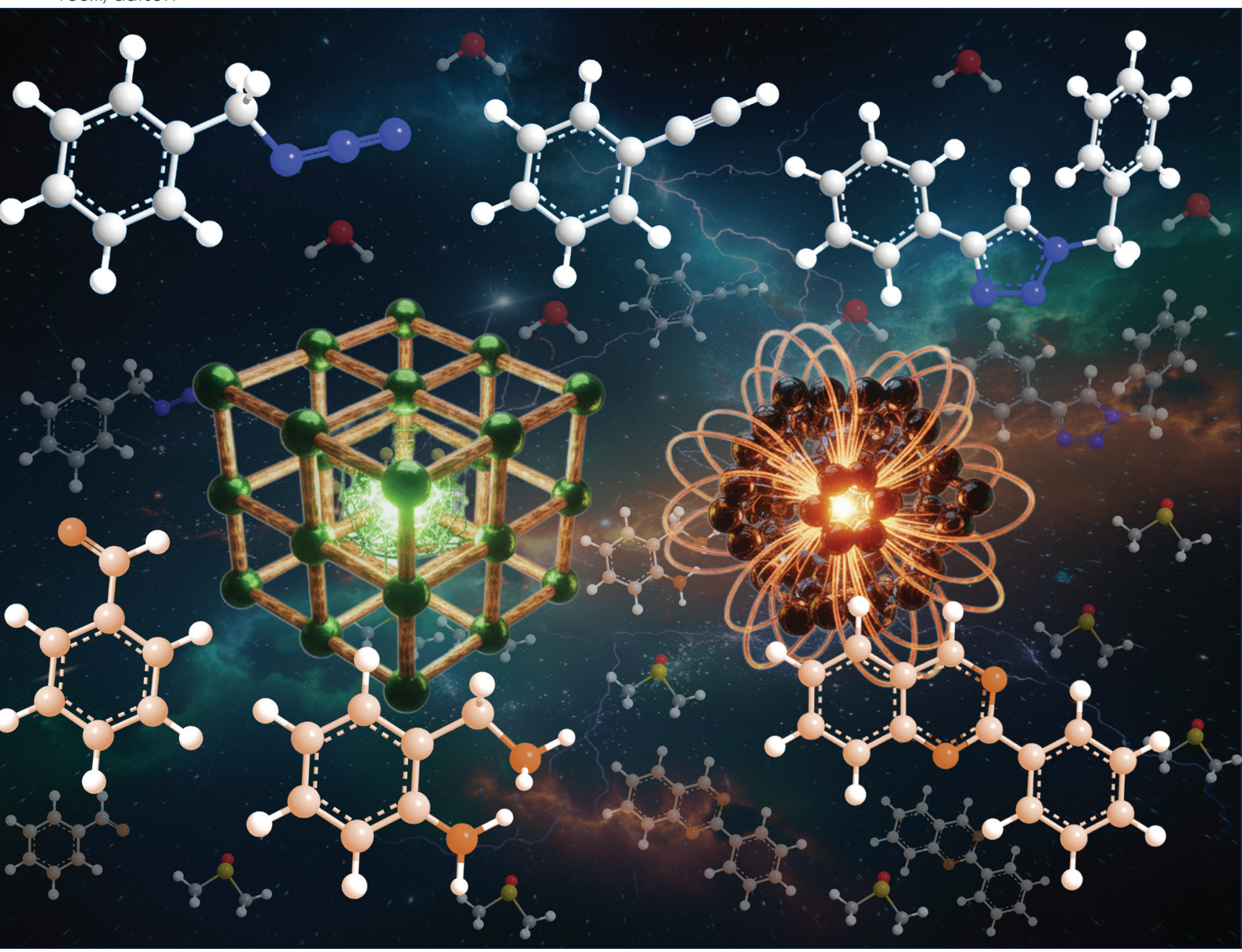

ISSN 1477-9226

ROYAL SOCIETY OF CHEMISTRY

PAPER

Kalyanjyoti Deori *et al.*

Interplay of morphology and particle size in CuBDC MOFs governing catalytic selectivity for the efficient synthesis of 1,4-disubstituted 1,2,3-triazoles and 2-substituted quinazolines

Dalton Transactions

ROYAL SOCIETY OF CHEMISTRY

PAPER

View Article Online
View Journal | View Issue

Check for updates

Cite this: *Dalton Trans.*, 2025, **54**, 17444

Published on 05 November 2025. Downloaded on 06.05.26 00:28:10.

Interplay of morphology and particle size in CuBDC MOFs governing catalytic selectivity for the efficient synthesis of 1,4-disubstituted 1,2,3-triazoles and 2-substituted quinazolines

Masshuda Madni Khatun, Priyanka Gogoi, † Nilakshi Dutta, † Puja Pokhrel, Diganta Sarma * and Kalyanjyoti Deori *

Even though metal–organic framework (MOF) materials are developing quickly, it is still very important to develop multifunctional MOFs with different sizes and morphological attributes and use them in catalytic applications. Cu based MOFs have garnered significant attention in the field of catalysis due to their high catalytic performance, cost effective synthesis and natural abundance of copper which make them easily accessible. Herein, we present an approach utilizing two Cu-based MOFs with distinct morphologies, synthesized *via* solvothermal (CuBDC-S) and reflux methods (CuBDC-O), as heterogeneous catalysts for the efficient synthesis of 1,4-disubstituted 1,2,3-triazoles (up to 98% yield) and 2-substituted quinazolines (up to 99% yield). The two different synthesis methods allowed us to modulate the morphology of the CuBDC (BDC-terephthalic acid) MOFs, thereby providing a unique opportunity to investigate the impact of structural differences on catalytic performance. Our results demonstrate that these MOFs, with their tailored morphologies, can significantly enhance catalytic activity under efficient conditions, offering good to excellent yields across a broad substrate range. CuBDC with a cubical morphology (CuBDC-O) synthesized by the reflux method exhibited higher efficiency in both catalytic reactions. Furthermore, to investigate the effects of morphology and other reaction parameters, two additional CuBDC MOFs were synthesised under modified conditions, one including a PVP assisted route (CuBDC-P) and another by an extended 24 h synthesis (CuBDC-M) while keeping the other parameters same as those of CuBDC-O. However, our findings reveal that none of the prepared catalysts could offer better yields as compared to CuBDC-O. This work represents the first report of utilizing morphology-controlled CuBDC MOFs for these two reactions, establishing a versatile and recyclable catalytic system. Our findings demonstrate the morphology transition in MOFs as a strategic tool for advancing heterogeneous catalysis in the synthesis of biologically important heterocycles.

Received 10th October 2025,
Accepted 5th November 2025

DOI: 10.1039/d5dt02446c

rsc.li/dalton

Introduction

In recent years, the design and synthesis of metal–organic frameworks (MOFs) have attracted considerable interest in the field of catalysis, particularly for the synthesis of heterocyclic compounds.[1–4] MOFs, composed of metal nodes coordinated with organic linkers, offer unique advantages such as high surface area, tunable pore structures, and diverse active sites.[5–8] Over the past decade, researchers have put significant efforts into developing various MOFs and looking into how they can be utilised for real life applications. These materials have shown their prominent potential across various fields including energy storage, environmental remediation, water splitting, biomedical science, developing sensors and boosting chemical reactions through catalysis.[9–14] Due to their aforementioned features, MOFs are marked as ideal candidates for heterogeneous catalysis, as they can provide robust catalytic platforms that blend the benefits of both homogeneous and heterogeneous systems. Their unique structural chemistry, where the metal clusters are well separated by the organic ligands helps in preventing catalyst deactivation, thus enhancing the catalytic efficiency.[15–20] However, conventional homogeneous catalysts, while highly effective in terms of chemo-, regio-, and enantioselectivity, often suffer from issues related to catalyst recovery and stability during reactions. To overcome these limitations, researchers have turned to MOFs, which not only offer the structural stability required for liquid-phase reactions but also present opportunities for catalyst recovery and reusability.[21–23]

Department of Chemistry, Dibrugarh University, Dibrugarh-786004, Assam, India. E-mail: kalchemdu@gmail.com, kalchemdu@dibru.ac.in, dsarma22@gmail.com, dsarma22@dibru.ac.in

† These authors contributed equally.

This journal is © The Royal Society of Chemistry 2025

Published on 05 November 2025. Downloaded on 06.05.26 00:28:10.

One of the emerging strategies to enhance the catalytic performance of MOFs lies in the morphology-controlled synthesis, which can significantly influence the exposure of crystal facets, distribution of active sites, and the availability of coordinatively unsaturated metal centers. By tailoring the morphology, MOFs can be engineered to display more accessible active sites, thus improving their catalytic activity. This morphological tuning is particularly crucial when the MOFs are employed in complex organic transformations, as it directly impacts the reaction kinetics and the interaction between the catalyst and the substrates.[24–27] Despite the progress in MOF synthesis, the exploration of their size and morphological effects in catalysis, especially for the synthesis of 1,4-disubstituted 1,2,3-triazoles and 2-substituted quinazolines, remains underexplored. Triazoles[28–31] and quinazolines[32–34] are highly valued in the pharmaceutical industry due to their diverse biological activities, including antibacterial, anti-inflammatory, and antitumor properties.[35,36] Over the past years a number of Cu based catalysts such as CuI,[37,38] Cu $(OAc)_2$,[39,40] CuMPS MOF,[41] CuBTC (benzene tricarboxylic acid) MOF,[42] and Fe_3O_4@SiO_2@Cu–MOF-74[43] were investigated for the synthesis of the bioactive moieties triazoles and quinazoline. However, the synthesis methods often require harsh conditions, expensive reagents, or extended reaction times, which limit their practicality.

Hence taking all these factors into account, we developed two CuBDC MOFs displaying distinct morphological features by solely changing the method of synthesis. Characterization techniques such as SEM, XPS, FTIR and XRD were employed to confirm the formation and morphological features of the synthesized MOFs. The primary novelty of our work lies in the rational design and utilization of a structurally well-defined Cu-based metal–organic framework (CuBDC) as a multifunctional heterogeneous catalyst for the sustainable synthesis of pharmaceutically important heterocycles, namely, 1,4-disubstituted 1,2,3-triazoles *via* azide–alkyne cycloaddition (AAC) reaction and 2-substituted quinazolines through oxidative coupling of 2-aminobenzylamine and benzaldehyde. Unlike most previously reported homogeneous or supported systems, our work demonstrates how size and morphological control in MOFs directly influences catalytic performance, offering mechanistic insight into structure–reactivity relationships. Among the various CuBDC samples synthesized, the CuBDC-O catalyst, with a particle size of 2 ± 0.5 μm and a homogeneous cubic morphology, most efficiently catalyzes both the mechanistically distinct organic transformations under efficient reaction conditions, demonstrating a level of multifunctionality rarely reported for MOFs. Additionally, the wide substrate scope and excellent recyclability of the catalyst are the potential striking features of our catalytic protocol.

Experimental section

Materials and reagents

Cupric chloride dihydrate ($CuCl_2{\cdot}2H_2O$, 99%, Sigma Aldrich), terephthalic acid (BDC, 99%, TCI), dimethyl formamide (DMF, 99%, SRL), methanol (CH_3OH, SRL, 99.8%), benzyl bromide (Spectrochem and TCI with 98% purity), sodium azide (NaN_3, 99%, Spectrochem), phenylacetylene (SRL, 98%), dimethylsulfoxide (DMSO, SRL,), 2-aminobenzylamine (Spectrochem), benzaldehyde (TCI, 99%,) and all the related substrates were purchased from Spectrochem with 98% purity. All chemicals were used as received without further purification. The organic substrates were isolated by column chromatography (60–200 mesh) over silica gel. Thin-layer chromatography was performed using silica gel 60 F_{254} plates and visualized under UV light.

Catalyst preparation

Synthesis of a CuBDC MOF by a solvothermal method. In a typical experimental procedure, 3 mmol of copper(II) chloride dihydrate ($CuCl_2{\cdot}2H_2O$) and 3 mmol of terephthalic acid (BDC) were added to 30 mL of DMF–ethanol (1 : 1 ratio) mixture in a round bottom flask and subjected to continuous magnetic stirring. After being stirred continuously for a period of 30 minutes, the homogenous solution was transferred to a Teflon-lined stainless-steel autoclave, maintained at 100 °C for 24 h. The obtained blue powder was isolated *via* centrifugation, washed with DMF and ethanol, and finally oven dried at 80 °C. This was represented as CuBDC-S.

Synthesis of a CuBDC MOF by reflux. Similarly, 3 mmol of copper(II) chloride dihydrate ($CuCl_2{\cdot}2H_2O$) and 3 mmol terephthalic acid (BDC) were added to 30 mL of DMF–ethanol (1 : 1) mixture taken in a 100 mL round bottom flask and the mixture was refluxed at 100 °C for 12 h with continuous magnetic stirring. The obtained blue powder was isolated *via* centrifugation, washed with DMF and ethanol, and finally oven dried at 80 °C. This sample was named CuBDC-O.

We also synthesised two other CuBDC MOFs, one by extending the synthesis duration of CuBDC-O to 24 hours, keeping all other reaction parameters constant (designated as CuBDC-M) and the other using PVP-assisted synthesis while maintaining identical parameters to those used for CuBDC-O, with a fixed metal precursor to PVP ratio of 3 : 1 (CuBDC-P).

Synthesis of azides

The azides were synthesized following a reported method.[31] In brief, to a solution of acetone–water mixture (3 : 1), 20 mmol of sodium azide (NaN_3) and 10 mmol of benzyl/substituted benzyl bromide were added. Depending on the type of azide, the mixture was stirred for 0.5–8 h, extracted with dichloromethane, washed with brine and then dried using anhydrous Na_2SO_4. Finally, it was concentrated under vacuum, to get the final benzyl azide/substituted benzyl azide.

Catalytic protocol for the synthesis of 1,4-disubstituted 1,2,3-triazoles

The impact of the morphological attributes of the synthesized copper MOFs in catalysis was tested for triazole synthesis. In brief, benzyl azide (0.38 mmol) and phenylacetylene (0.46 mmol, 1.2 equiv.) were taken in a round bottom flask. To it, an H_2O–ethylene glycol mixture (30 : 1 ratio) and 10 mg (0.02 mmol) of the as-synthesized CuBDC-O or CuBDC-S were

Published on 05 November 2025. Downloaded on 06.05.26 00:28:10.

added and the whole reaction mixture was stirred at room temperature over a period of time. The progress of the reaction was monitored using TLC under UV light irradiation. Upon completion of the reaction, the product was extracted using ethyl acetate and dried using anhydrous Na_2SO_4. Under reduced pressure the organic solvent was evaporated. The desired product was then purified by performing column chromatography over silica gel using a mixture of ethyl acetate and hexane, and characterised using ^1H and ^{13}C NMR taking $CDCl_3$ as NMR sampling solvent.

Synthesis of 2-substituted quinazolines *via* coupling of 2-aminobenzylamine with benzaldehyde

In a round bottom flask, 0.1 mmol 2-aminobenzylamine and 0.12 mmol benzaldehyde were taken. To this, 2 mL of DMSO and 15 mg (0.03 mmol) of the synthesized CuBDC catalyst were added and stirred at 60 °C in air. Using TLC under UV irradiation, the reaction progress was monitored. After completion of the reaction, the mixture was cooled to room temperature and extracted using ethyl acetate. After that, the organic layer was dried using anhydrous Na_2SO_4 and concentrated under vacuum. Using a mixture of ethyl acetate and hexane, the desired product was isolated and purified by performing column chromatography over silica gel. The obtained products were characterised using ^1H and ^{13}C NMR taking $CDCl_3$ as NMR sampling solvent.

Instrumentation

Powder X-ray diffraction (XRD). XRD measurements were carried out with a Bruker D8 Advance X-ray diffractometer using monochromatic Cu Ka radiation (l $\frac{1}{4}$ 1.54056 A).

Scanning electron microscopy. Scanning electron microscopy with energy dispersive X-ray spectroscopy (SEM-EDAX) analysis was carried out on a Jeol 6390LA/Oxford XMX N instrument with the accelerating voltage ranging from 0.5 to 30 kV and equipped with a tungsten filament.

UV-visible absorption spectroscopy. The sample was dispersed in ethanol by ultrasonication. UV-visible absorption measurements were conducted on a Shimadzu UV-1700 UV-vis spectrophotometer.

Fourier transform infrared (FTIR) spectroscopy. To obtain the FTIR spectra (4000–400 cm^{-1}), a PerkinElmer FTIR 2000 spectrophotometer was employed.

Nuclear magnetic resonance (NMR). A Bruker Ascend 500 MHz spectrophotometer was used to record ^1H and ^{13}C NMR spectra at 500 MHz and 125 MHz, respectively.

X-ray photoelectron spectroscopy (XPS). XPS measurements were carried out using a PHI 5000 Versa Probe III electron spectrometer from Physical Electronics. The binding energies of the obtained XPS spectra were corrected with reference to the C(1s) standard peak at 284.6 eV.

Thermogravimetric analysis. The thermal stability of the prepared samples was analysed on a Mettler Toledo TGA/DSC 1 STARe analyzer.

Photoluminescence spectroscopy (PL). Room temperature photoluminescence (RT-PL) analysis was performed on homogeneously dispersed samples using a Horiba Fluoromax integrated compact benchtop spectrofluorometer with a lifetime attachment.

Brunauer–Emmett–Teller (BET). The surface area and pore sizes of the as-synthesised samples were determined using the BET equation with the help of a Quantachrome NovaWin at 77 K.

Results and discussion

The XRD patterns of CuBDC-O and CuBDC-S are shown in Fig. 1. The major diffraction peaks are observed at 2θ values of 10.3°, 12.2°, 13.6°, 17.1°, 20.6°, 24.8°, 34.1° and 42.1°. These peaks are attributed to the (110), (020), (11$\bar{1}$), (20$\bar{1}$), (111), (220), ($\bar{4}$02) and (242) planes of CuBDC, respectively, indicating that the synthesized Cu MOFs using solvothermal and reflux methods are consistent with the known structure of the standard one.[44] Although CuBDC-S and CuBDC-O share the same crystal structure, their distinct morphologies influence local ordering and facet exposure. CuBDC-S, with a mixed cubic/flower-like morphology, contains multiple crystal facets and stacking faults, resulting in broadened peaks without additional reflections, closely matching the reference pattern. In contrast, CuBDC-O, with a uniform cubic morphology, exhibits enhanced crystallinity and preferential facet orientation, which lead to the appearance of additional weak peaks at 2θ = 13° and 19°. Such morphology-dependent changes in XRD patterns have been reported in other Cu–BDC systems, where the crystal shape and growth direction alter facet exposure and ordering without changing the overall framework topology.[45,46] Nevertheless the dominant reflection matches well with the reported CuBDC pattern, thereby validating the formation of the targeted MOF structure. Also, upon closer inspection, subtle differences in the intensities of specific peaks, as well as in the intensity ratios between peaks, are observed in the XRD patterns. These variations reflect differences in the preferred crystal orientation and the relative abundance of exposed crystal facets arising from morphological changes rather than alterations in the crystal phase itself. Such intensity modulation without any shift in 2θ values has also been reported in other MOFs such as MOF-74 and ZIF-8, where morphological transitions affected peak intensity but not lattice periodicity.[47,48]

The FTIR spectral outputs of the synthesized MOFs *viz.* CuBDC-O and CuBDC-S are shown in Fig. 1b. Several IR bands within the 1200–1000 and 1000–700 cm^{-1} ranges were attributed to the in-plane and out-of-plane C–H bending modes. The observed absorption peak at 1667 cm^{-1} was slightly lower than that of the usual stretching vibration frequency of C=O in the terephthalic acid spectrum, which is typically at 1684 cm^{-1}.[49] This discrepancy is attributed to the deprotonation of the carboxylic acid group of 1,4-benzenedicarboxylic acid (BDC) during the synthesis. C=C corresponded to 1512 cm^{-1}, and symmetric and asymmetric O–C–O stretching was assigned at 1395 and 1576 cm^{-1}, respectively.[50] The separation between

 This journal is © The Royal Society of Chemistry 2025

Published on 05 November 2025. Downloaded on 06.05.26 00:28:10.

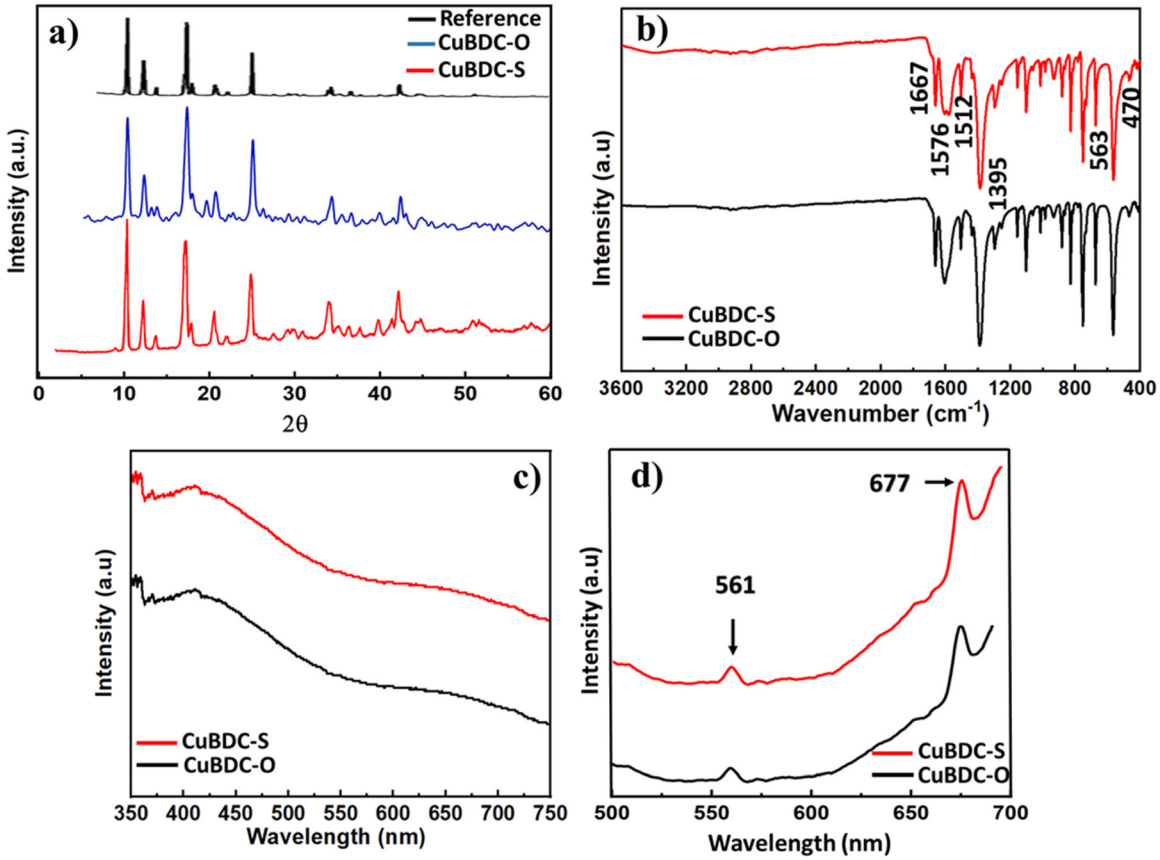

Fig. 1 (a) PXRD patterns of CuBDC-S, CuBDC-O and reference, (b) FTIR spectra of CuBDC-S and CuBDC-O, (c) UV spectra of CuBDC-O and CuBDC-S, and (d) PL spectra of CuBDC-O and CuBDC-S.

the two modes (symmetric and asymmetric) is a suggestive indication that the carboxylate group (COO) of the BDC ligand binds to the metal *via* a bidentate mode.[51] Moreover, the stretching vibration signals corresponding to Cu–O identified at 470 and 563 cm^{-1} confirm the successful development of CuBDC MOFs.[52]

The UV-visible absorption spectra of the synthesised CuBDC MOFs are shown in Fig. 1c. The absorption band in the UV–Vis spectrum of CuBDC in the range of 380–450 nm arises primarily from ligand-to-metal charge transfer (LMCT) transitions between the carboxylate oxygen (ligand) and Cu^{2+} centers, which are characteristic of Cu-based MOFs. The weak shoulder or low-intensity broad feature in the visible region between 600 and 700 nm is attributed to intra-configurational d–d transitions characteristic of Cu^{2+} ions in a distorted square-planar environment, consistent with previously reported Cu-based MOFs.[53] When excited at a wavelength of 409 nm, the CuBDC MOF shows two emission peaks at 561 and 677 nm (Fig. 1d). This emission indicates the good interaction between the metal centre and the organic ligands and thus the influence of its framework on electronic properties.

The morphological characteristics of the synthesised CuBDC MOFs were examined using scanning electron microscopy as shown in Fig. 2. The Cu MOFs produced using reflux and solvothermal techniques exhibit a homogeneous cubical type and mixed morphology (hierarchical flower like along with a cubical type) with a particle size of 2 ± 0.5 μm and 20 μm, respectively. The successful synthesis of the CuBDC MOFs was also confirmed by EDX analysis reflecting the presence of copper, carbon and oxygen in the samples (Fig. 2g and h). Furthermore, the elemental mapping of the synthesised materials indicates the uniform distribution of all the constituent elements across the CuBDC-O (Fig. S1(b–d), SI) and CuBDC-S (Fig. S1(f–h), SI) structures.

The thermal stability of the synthesized MOFs was assessed by thermogravimetric analysis, where two distinct weight losses are visible for both CuBDC-O (Fig. 3a) and CuBDC-S (Fig. 3b). The removal of absorbed water and some leftover DMF is responsible for the initial weight loss at 170 °C–210 °C. In accordance with earlier reports, the second weight loss step in the range of 220 °C to 440 °C is associated with ligand breakdown *i.e.* decomposition of BDC and copper oxide formation. However, it is seen that CuBDC-O exhibited its last major degradation step at 435 °C, slightly higher than that of CuBDC-S (425 °C). Beyond this temperature, both the curves reached a plateau, suggesting complete degradation of the framework and presence of stables residue. The difference in degradation temperature reflects the influence of morphology

Published on 05 November 2025. Downloaded on 06.05.26 00:28:10.

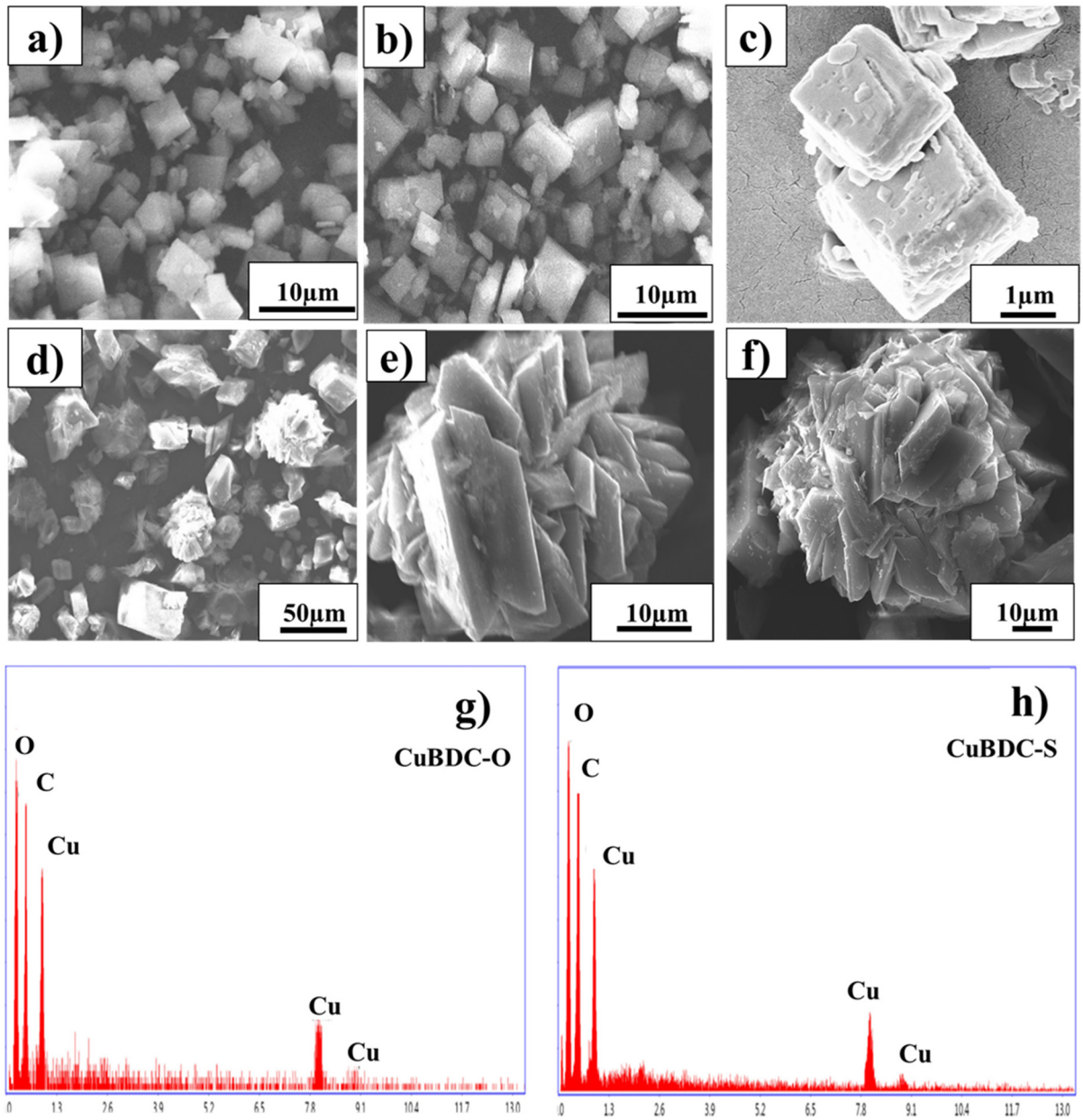

Fig. 2 SEM images of (a–c) CuBDC-O and (d–f) CuBDC-S and SEM-EDS spectra of (g) CuBDC-O and (h) CuBDC-S.

on thermal stability, revealing that CuBDC-O is slightly more stable than CuBDC-S.

The chemical composition of the as-synthesized MOFs was examined by XPS analysis. Fig. 4a and e present the broad survey spectrum of CuBDC-O and CuBDC-S, respectively, revealing the presence of Cu 2p along with C 1s and O 1s states in the samples. The high-resolution Cu (2p) spectrum for both MOFs (Fig. 4b and f) show two distinct peaks at binding energies 934.8 eV and 954.8 eV corresponding to Cu $2p_{3/2}$ and Cu $2p_{1/2}$ respectively, which is in good agreement with earlier literature reports. According to literature reports, the Cu $2p_{3/2}$ and Cu $2p_{1/2}$ peaks must differ by 20 eV, which is also the case in our study.[54] Furthermore, the presence Cu^{2+} in the samples is confirmed by the presence of two satellite peaks in the 940–945 eV range.[55,56] Fig. 4c and g show the high resolution XPS spectra for C 1s of CuBDC-O and CuBDC-S, respectively, exhibiting two peaks at 284.7 and 288.8 eV corresponding to the sp^2-bonded carbon of carboxyl and phenyl groups.[57] The XPS spectra of O 1s for both the copper MOFs exhibit a binding energy peak at 532.1 eV, which is consistent with the standard value (Fig. 4d and h).[58] However significantly different signal-to-noise S/N ratios in the broad survey spectra of XPS (Fig. 4a *vs.* e) are observed due to several key factors such as the dwell time, surface properties and surface elemental availability of the two morphologies. In CuBDC-S, the presence of mixed cubic and hierarchical flower-

 This journal is © The Royal Society of Chemistry 2025

Published on 05 November 2025. Downloaded on 06.05.26 00:28:10.

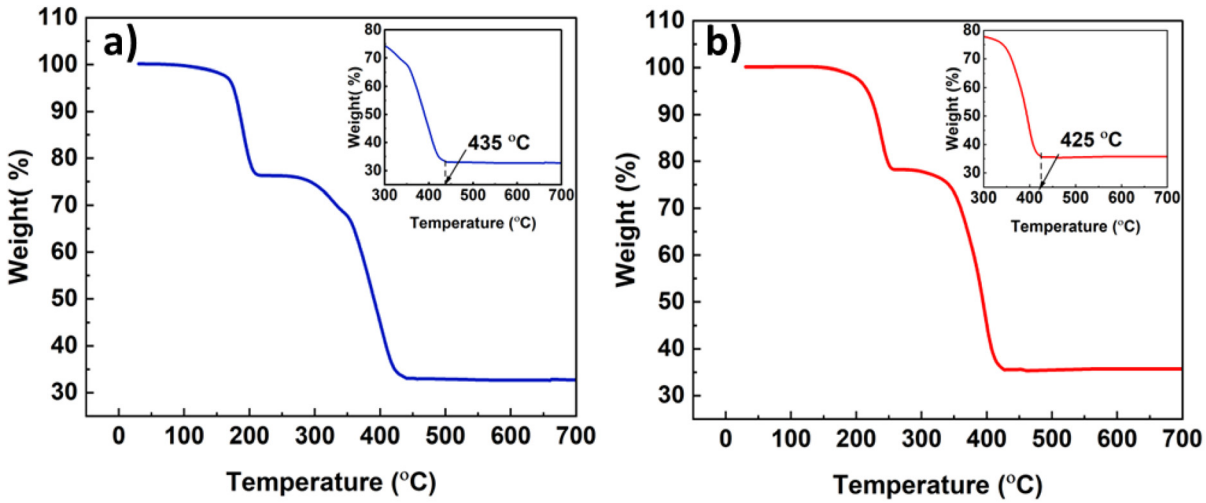

Fig. 3 TGA graphs of (a) CuBDC-O and (b) CuBDC-S.

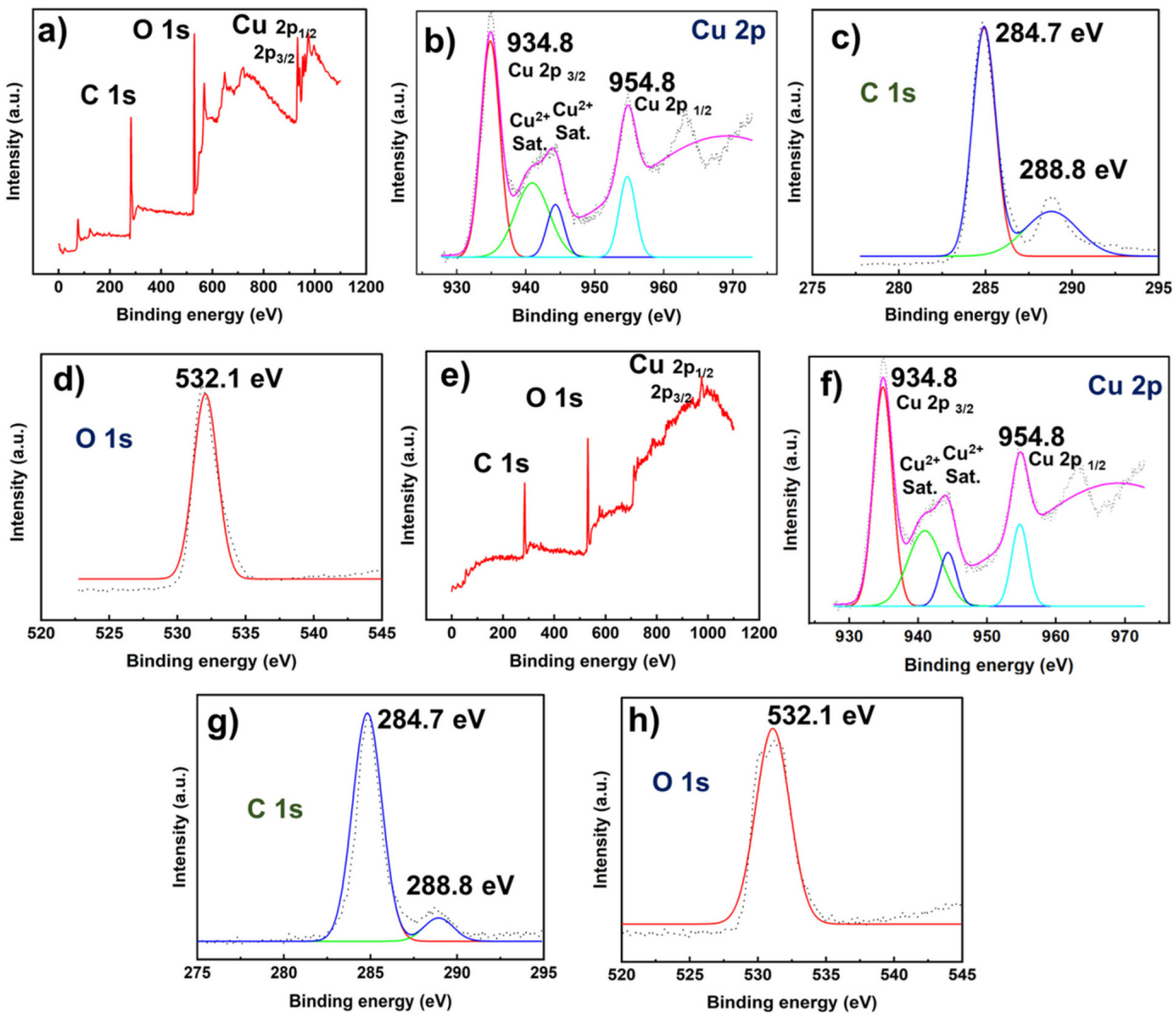

Fig. 4 XPS wide survey spectra of (a) CuBDC-O; CuBDC-O high resolution XPS spectra of (b) Cu 2p, (c) C 1s and (d) O 1s; XPS wide survey spectra of (e) CuBDC-S; and CuBDC-S high resolution XPS spectra of (f) Cu 2p, (g) C 1s and (h) O 1s.

Published on 05 November 2025. Downloaded on 06.05.26 00:28:10.

like structures introduces multiple crystal facets and increased surface roughness, leading to non-uniform surface termination. As a result, many Cu sites become partially buried within interlayer regions, reducing their effective exposure to the X-ray beam.[59] This limited surface accessibility, combined with increased electron scattering from rough surfaces, attenuates photoelectron signals and lowers the S/N ratio. Conversely, CuBDC-O with its uniform cubic morphology offers a smoother surface and greater exposure of Cu centers, enabling stronger and clearer signals in the survey spectrum.

The textural features of the synthesized composite and average pore diameters were examined *via* the Brunauer–Emmett–Teller (BET) and BJH methods (Fig. 5). Nitrogen adsorption–desorption isotherms (Fig. 5a) were employed to determine the surface area and pore characteristics of CuBDC-O and CuBDC-S. The isotherm exhibits a hybrid profile between type I and type IV, indicative of a coexistence of microporous and mesoporous domains. In compliance with IUPAC guidelines for accurate pore structure evaluation, the total pore volume was computed from the adsorption data at a relative pressure close to saturation (p/p_0 = 0.99). The BET surface areas of CuBDC-O and CuBDC-S were found to be 58.889 $m^2\ g^{-1}$ and 40.937 $m^2\ g^{-1}$, respectively, with corresponding total pore volumes of 0.067 $cm^3\ g^{-1}$ and 0.038 $cm^3\ g^{-1}$.

In order to study the effect of the transitional morphological properties of the as-synthesized CuBDC samples in catalysis, azide–alkyne cycloaddition (AAC) reaction was carried out. A series of experiments were conducted using benzyl azide (**1a**) and phenyl acetylene (**2a**) as model substrates at room temperature. The regioselective formation of 1,2,3-triazole with high yield (98%) was attained using CuBDC–O as the catalyst (Table 1, entry 2), while CuBDC-S resulted in 70% yield (Table 1, entry 5) under the same reaction conditions even after 4 h. Furthermore, extending the reaction time for CuBDC-S beyond 4 h *i.e.* for 7 h did not lead to any significant improvement in product yield (Table 1, entry 6). Hence all the reaction conditions are then optimised using CuBDC-O

Table 1 Optimization of reaction conditions[a] of 1,4-disubstituted 1,2,3-triazoles

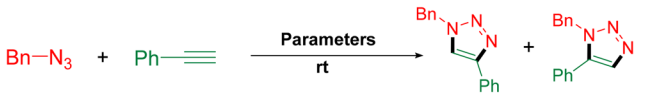

1a 2a 3aa 4aa

Entry	Catalyst	Temperature	Time (h)	Yield[b] (%) 3aa	4aa
1	CuBDC-O	rt	1	80	0
2	CuBDC-O	rt	2	98	0
3	CuBDC-S	rt	2	Trace	0
4	CuBDC-O	rt	3	98	0
5	CuBDC-S	rt	4	70	0
6	CuBDC-S	rt	7	75	0
7	CuBDC-P	rt	2	Trace	0
8	CuBDC-M	rt	2	60	0

[a] Reaction conditions: **1a** (0.38 mmol), **2a** (0.46 mmol, 1.2 equiv.), CuMOF (10 mg, 0.02 mmol), and H_2O/EG (3.0 mL/0.1 mL) at rt. [b] Isolated yield. Bn, benzyl.

(Table 2). The reaction resulted in the best yield of the desired product in air for 2 h using water along with a few drops of ethylene glycol as the reaction medium (Table 2, entry 4). The higher yield of the desired product using CuBDC-O as a catalyst can be attributed to its homogeneous cubic morphology with a particle size around 2 ± 0.5 μm which is less than that of CuBDC-S (20 μm). Also, the greater BET surface area of CuBDC-O (compared to CuBDC-S) is a direct consequence of its smaller particle size, which provides a larger exterior surface to volume ratio. This results in a greater number of exposed active sites, and shorter diffusion paths, thereby facilitating better reactant interaction and electron transfer during the reaction, ultimately enhancing product yield. Furthermore, MOFs with smaller particle sizes typically exhibit lower diffusion barriers and more efficient substrate and product

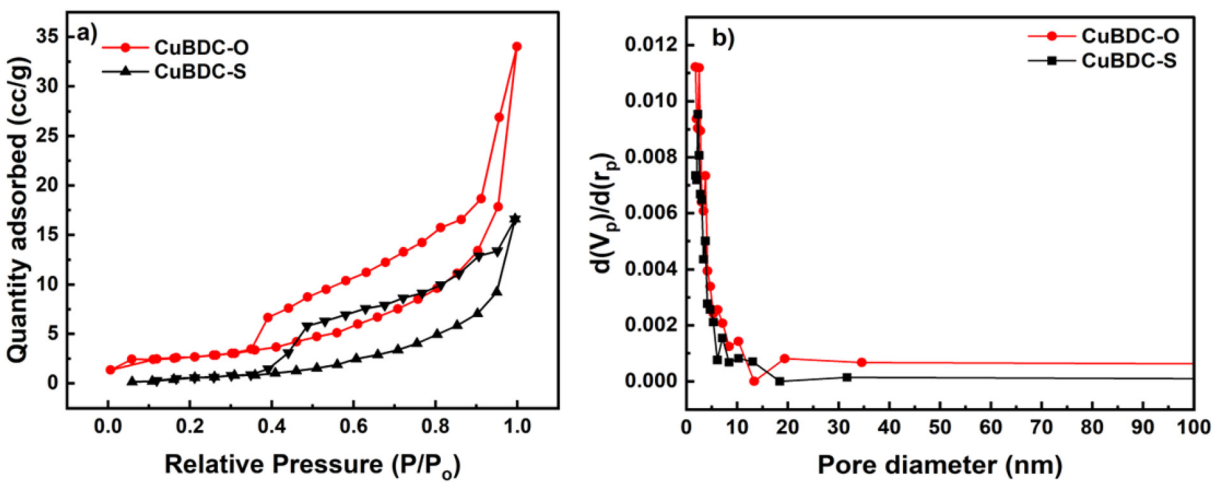

Fig. 5 (a) N_2 adsorption/desorption isotherm and (b) BJH pore size distribution of CuBDC-O and CuBDC-S.

This journal is © The Royal Society of Chemistry 2025

Published on 05 November 2025. Downloaded on 06.05.26 00:28:10.

Table 2 Solvent effects[a] on the synthesis of 1,4-disubstituted 1,2,3-triazoles from benzyl azide (**1a**) and phenylacetylene (**2a**)

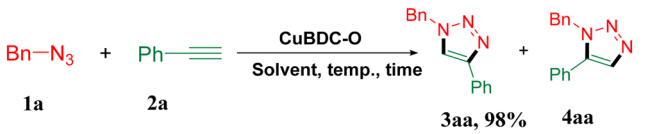

1a **2a** **3aa, 98%** **4aa**

Entry	Solvent	Temperature	Time (h)	Yield[b] (%) 3aa	4aa
1	No solvent	rt	2	67	—
2	H_2O only	rt	2	85	—
3	EG only	rt	2	60	—
4	**H_2O : EG**	**rt**	**2**	**98**	—
5	H_2O : EG	rt	3	98	—
6	DMF	rt	2	76	—
7	DCM	rt	2	71	—
8	CH_3CN	rt	2	80	—
9	Toluene	rt	2	Trace	—
10	$CHCl_3$	rt	2	Trace	—
11	H_2O : EG	60 °C	2	75	15
12	H_2O : EG	80 °C	2	60	20
13	DMF	60 °C	2	50	15

[a] Reaction conditions: **1a** (0.38 mmol), **2a** (0.46 mmol, 1.2 equiv.), CuBDC-O (10 mg, 0.02 mmol), and H_2O/EG (3.0 mL/0.1 mL) at rt under air for 2 h. [b] Isolated yield. Bn, benzyl.

distribution through their pores, which results in higher catalytic activity.[60] In contrast, CuBDC-S with its mixed morphology likely possesses buried active sites within the interlayers, limiting surface accessibility and consequently reducing catalytic efficiency.

To further probe morphology-controlled effects, we conducted additional synthesis experiments under modified conditions. We attempted a PVP-assisted synthesis while maintaining identical parameters to those used for CuBDC-O, with a fixed metal precursor to PVP ratio of 3 : 1, aiming to direct the formation of a uniform hierarchical flower-like morphology. However, the resulting material, designated as CuBDC-P, did not exhibit any well-defined or distinct morphological features under the applied conditions, as evidenced by the SEM images (Fig. S2(a–c)). In a separate attempt to induce controlled morphological variation, we extended the synthesis duration of CuBDC-O to 24 hours, keeping all other reaction parameters constant. This modification facilitated the partial evolution of hierarchical features, and the resulting material, termed CuBDC-M, displayed an intermediate morphology between cubic and flower-like structures (Fig. S2(d–f)).

Both CuBDC-P and CuBDC-M were subsequently evaluated for their catalytic activity in the room-temperature synthesis of 1,4-disubstituted 1,2,3-triazoles, and the results are summarized in Table 1. CuBDC-P exhibited negligible catalytic efficiency, likely due to its poorly defined morphology, emphasizing the importance of structural order in catalytic function (Table 1, entry 7). Conversely, CuBDC-M showed moderate activity, achieving a product yield of 60% within 2 hours, which was still inferior to that of CuBDC-O (Table 1, entry 8). These findings collectively demonstrate that morphological control exerts a tangible influence on catalytic performance, complementing the size and surface area effects discussed earlier.

With the best solvent in hand *i.e.* H_2O/EG (ethylene glycol) for the reaction system (showing 98% yield), additional investigation on the effects of other solvents was carried out. When compared to non-polar solvents (Table 2, entry 9), the yield is relatively higher in moderately polar solvents (Table 2, entries 2–5), indicating that the substrates are effectively soluble in polar solvents. The $-N_3$ group present in azide shows good coordination with the two-hydroxyl group of ethylene glycol, thus creating the right conditions for all the reactants to be in the same phase.[31,61] A few drops of ethylene glycol functioned as a co-solvent, encouraging better collisions of the reactants, thus aiding in homogenising the reaction mixture, increasing yield (Table 2, entry 4), outperforming all other solvents. The reaction was also carried out with EG as the only solvent to ensure further confirmation and it was observed that a yield of only 60% was achieved within 2 h (Table 2, entry 3). An increase in temperature resulted in the formation of both isomers, which can be explained based on the fact that at high temperature thermal effects outweigh the catalytic effect, thus disrupting the regioselectivity of the reaction (Table 2, entries 11–13). Using 10 mg (0.02 mmol) of the catalyst (Table S1, entry 4, SI) resulted in optimum yield of the product, while reducing the catalyst loading resulted in lower yields (Table S1, entries 2, 3, 11 and 12, SI). We also performed the reaction in the absence of the catalyst while maintaining all other parameters constant, resulting in no formation of any product (Table S1, entry 1, SI). We also tested the reaction using the precursors $CuCl_2{\cdot}2H_2O$ and terephthalic acid separately and a physical mixture of these precursors (1 : 1); however, none of them produced higher yields than the as-synthesized CuBDC-O (Table S1, entries 8–10).

A sequence of reactions involving different substituted azides and aliphatic and aromatic terminal alkynes (Table 3) were performed after establishment of the optimal reaction conditions in order to assess the effectiveness of the created catalytic system. With good to excellent yields, the optimised catalytic conditions afforded a wide range of single isomeric products, 1,2,3-triazoles, possessing both electron donating and electron withdrawing substituents (Table 3, **3aa–3fh**). The most reactive among all the azides was discovered to be benzyl azide and substituted benzyl azide as they participated in the cyclization process with ease. Lower yields of products is observed from azides with strong electron donating groups (Table 3, **3ac–3ad**) as compared to those of azides with electron withdrawing groups (Table 3, **3ba–3da**). The position of the substituent on the azide, either at *m*- or *p*- position, was found to have a negligible effect on the cycloaddition. Similarly, several terminal alkynes were used to investigate the substituent effect on alkynes. Almost all alkynes exhibited a straightforward transition to the intended product, regardless of the type of functional group that was attached. Excellent tolerance to heterocyclic alkynes (Table 3, **3ff**) was achieved by this pro-

Published on 05 November 2025. Downloaded on 06.05.26 00:28:10.

Table 3 Substrate scope of CuBDC-O for the synthesis of 1,4-disubstituted 1,2,3-triazoles [a,b,c,d,e]

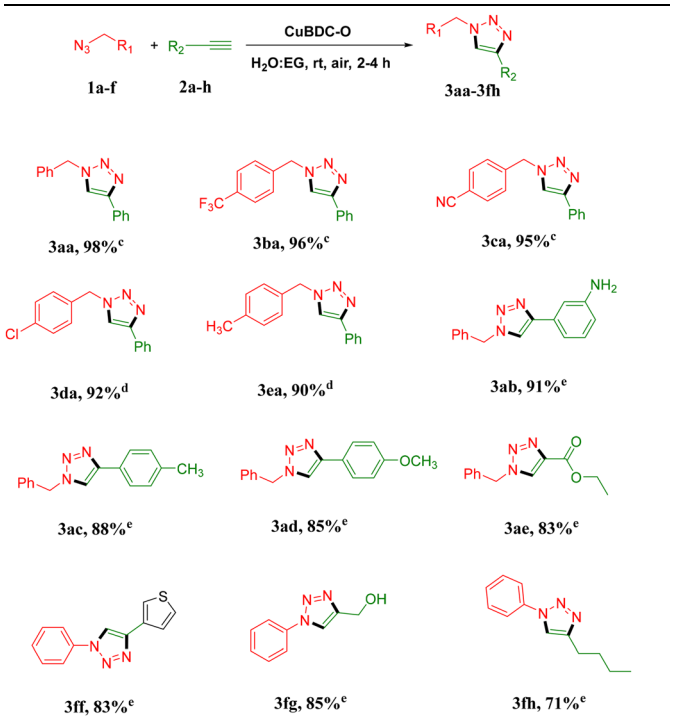

[a] Reaction conditions: azides (0.38 mmol), alkynes (0.46 mmol, 1.2 equiv.), CuBDC-O (10 mg, 0.02 mmol), and H_2O/EG (3.0 mL/0.1 mL) at rt under air. [b] Isolated yield. [c] 2 h. [d] 3 h. [e] 4 h.

tocol which supports the broad applicability of our catalytic system.

The effect of our CuBDC-O catalyst has been compared with those of other Cu catalysts in the azide–alkyne cycloaddition reaction in order to demonstrate the merit of the present study compared to previously reported ones (Table S3, SI).

A proposed reaction mechanism for the 1,3-dipolar cycloaddition reaction in the presence of the CuBDC-O catalyst was made based on the literature (Fig. 6).[62,63] In the coordinated structure, Cu(II) was present which functioned as a Lewis acid and catalysed the synthesis of 1,2,3-triazoles and its derivatives. Based on this, the Cu intermediate (**I**) is created in the first step by coordinating the phenyl acetylene to the Cu centres in the MOF structures. In the next step the proton from the acetylene group is abstracted and metal acetylide is formed (**II**). Subsequently benzyl azide attacks the previously formed Cu intermediate (**II**) and the final product is formed following a straightforward intramolecular cyclization.

Following encouraging outcomes from the synthesis of 1,4-disubstituted 1,2,3-triazoles the viability and applicability of the as-synthesized CuBDC-O and CuBDC-S were investigated for the synthesis of quinazoline also, *via* coupling of 2-aminobenzylamine and benzaldehyde. A series of reactions using 2-aminobenzylamine (**1a′**) and benzaldehyde (**2a′**) as the model substrates were carried out in order to ascertain the ideal reaction conditions (Table 4).

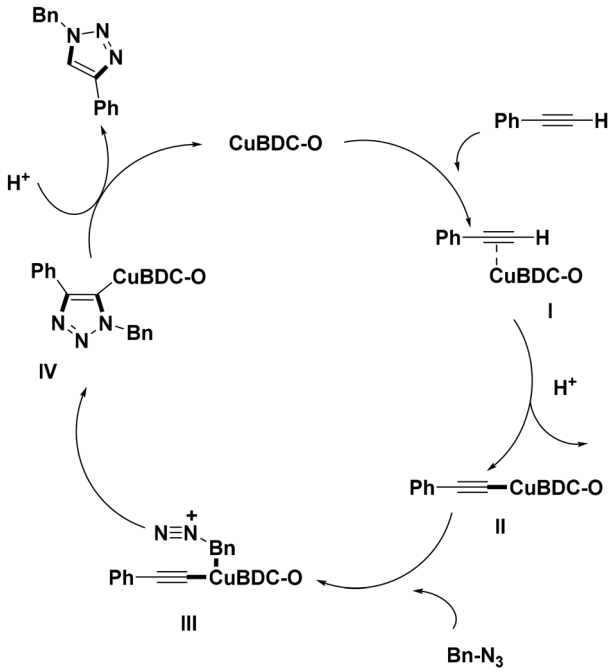

Fig. 6 The proposed mechanism for the synthesis of 1,2,3-triazoles in the presence of the CuBDC-O catalyst.

Several parameters were evaluated including catalysis time, solvent, temperature and catalyst loading. The reaction was initially conducted using 15 mg (0.03 mmol) of CuBDC-O in DMSO at room temperature, affording no results even after 24 h (Table 4, entry 1). However, on increasing the temperature to 60 °C, the reaction afforded the desired product in 99% yield within 10 h (Table 4, entry 2), which showed the effect of temperature on the reaction. Unlike the formation of triazoles that proceeded at room temperature, an elevated temperature was required herein because of higher requirement of activation energy for condensation of 2-aminobenzylamine and benzaldehyde, which involves multiple reaction steps. On further increasing the temperature to 80 °C, there was no notable difference in yield (Table 4, entry 3). On the other hand, lowering of temperature (50 °C, 40 °C) resulted in lower yield of the product (Table 4, entries 4 and 5). The reaction did not proceed under neat conditions (Table 4, entry 6) and yielded less product in polar protic solvents like methanol and ethyl acetate (Table 4, entries 9 and 10). The conversion of reactants into products was observed among different available solvents (Table 4), with DMSO being considered the ideal solvent medium producing the highest yield (99%) of the desired product (**3a′a′**) after 10 h at 60 °C in air (Table 4, entry 2).

The highest yield of the product was found when 15 mg (0.03 mmol) of the catalyst (Table S2, entry 3, SI) was used, while lowering the catalyst loading resulted in decreased yield of the product (Table S2, entries 2 and 10, SI). The requirement of a slightly higher catalyst amount (15 mg) for quinazoline synthesis compared to that for AAC reaction can be attributed to the higher activation energy and elevated temperature

 This journal is © The Royal Society of Chemistry 2025

Published on 05 November 2025. Downloaded on 06.05.26 00:28:10.

Table 4 Optimization of reaction parameters for the synthesis of 2 substituted quinazoline [a,b]

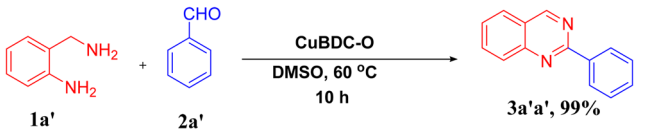

Entry	Solvent	Temperature	Time (h)	Yield[b] (%)
1	DMSO	rt	24	—
2	**DMSO**	**60 °C**	**10**	**99%**
3	DMSO	80 °C	10	99%
4	DMSO	50 °C	10	50%
5	DMSO	40 °C	10	50%
6	Neat	60 °C	10	—
7	H_2O	60 °C	10	60%
8	PEG-400	60 °C	10	55%
9	Methanol	60 °C	10	40%
10	Ethyl acetate	60 °C	10	40%
11	DMSO	60 °C	6	Trace
12	DMSO	60 °C	8	50%

[a] Reaction conditions: 2-aminobenzylamine (0.1 mmol), benzaldehyde (0.12 mmol), CuBDC-O (15 mg, 0.03 mmol), and DMSO (2 mL). [b] Isolated yield.

Table 5 Substrate scope of CuBDC-O for the synthesis of 2-substituted quinazoline

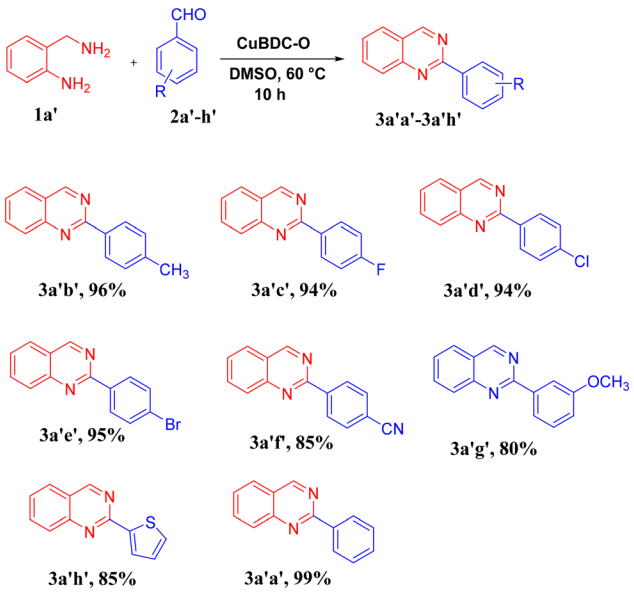

(60 °C) needed for this reaction. Furthermore, since the quinazoline synthesis involves multistep condensation and oxidative cyclization processes, a greater number of active sites are required to facilitate it efficiently. The reaction yielded no product in the absence of a catalyst (Table S2, entry 5, SI). In order to test the usefulness of the synthesized catalyst, we also carried out the reaction with other variants such as individual $CuCl_2{\cdot}2H_2O$ and terephthalic acid and a a physical mixture of these two (1 : 1), while keeping all other parameters constant, and none yielded better results as compared to CuBDC-O (Table S2, entries 7–9). To study the effect of the morphological behaviour of the MOF in coupling of 2-aminobenzylamine and benzaldehyde to form quinazoline, we expanded the catalytic protocol by replacing the catalyst with CuBDC-S (Table S2, entry 6, SI). As a result, the yield of the desired product (**3a′a′**) obtained was 75%. Lower yield of **3a′a′** can be assigned to the formation of a mixed morphology in CuBDC-S, reducing the amount of exposed surface area, thereby blocking the active sites of Cu. As a consequence, the diffusion of reactant molecules was hindered resulting in decreased yield of the desired product.

After the optimal conditions were determined, substituted benzaldehydes were added for analyses to confirm the protocol's functional group tolerability. Different aldehydes reacted with 2-aminobenzylamine to afford the expected 2-substituted quinazolines in good to excellent yields, regardless of the electronic effect of the substituent in the aromatic ring. Table 5 provides a summary of the findings.

A proposed mechanism for the synthesis of 2-substituted quinazoline using CuBDC-O as a catalyst is shown in Fig. 7 in accordance with experimental findings (BET, XPS and SEM) and previous literature reports. The larger surface area, abundance of coordinatively unsaturated Cu^{2+} sites, and the presence of oxygen atoms from the carboxylate linkers in CuBDC-O collectively facilitate the oxidative cyclization pathway, thereby promoting the efficient formation of quinazolines. At first the exposed Cu^{2+} sites in CuBDC-O interact with the –CO group of benzaldehyde, thus functioning as a Lewis acid and activating benzaldehyde. The activated benzaldehyde (**I**) then reacts with 2-aminobenzylamine to form an intermediate (**II**), which then further undergoes intramolecular cyclization to form **III**. Finally intermediate **III** is rapidly oxidized in the presence of ambient oxygen, catalysed by the exposed Cu^{2+} sites, thus resulting in the desired quinazoline product (**4**).[64]

The catalytic performance observed in the formation of quinazoline was compared with those in previously reported works (Table S4, SI). The earlier reports revealed the use of high temperature and bases, yet the product yield was less, while it was observed that our suggested catalytic system proceeded without the aid of a base and at lower temperature producing good to excellent yields and hence was advantageous.

In order to investigate the effectiveness of the catalyst and access its sustainability, a recyclability test was carried out. For the reusability of the as-synthesized catalyst for 1,4-disubstituted 1,2,3-triazole synthesis, benzyl azide and phenylacetylene were chosen as model substrates. For 2-substituted quinazoline synthesis, 2-aminobenzylamine and benzaldehyde were chosen to examine recyclability. Following the reactions, the catalyst was removed from the reaction vessel *via* centrifugation, washed with ethanol, dried and then used for four consecutive cycles following the same procedure. In both the organic transformations the CuBDC-O catalyst delivers significantly higher yields and faster reaction rates than other reported MOF and oxide catalysts, attributed to its optimized

Published on 05 November 2025. Downloaded on 06.05.26 00:28:10.

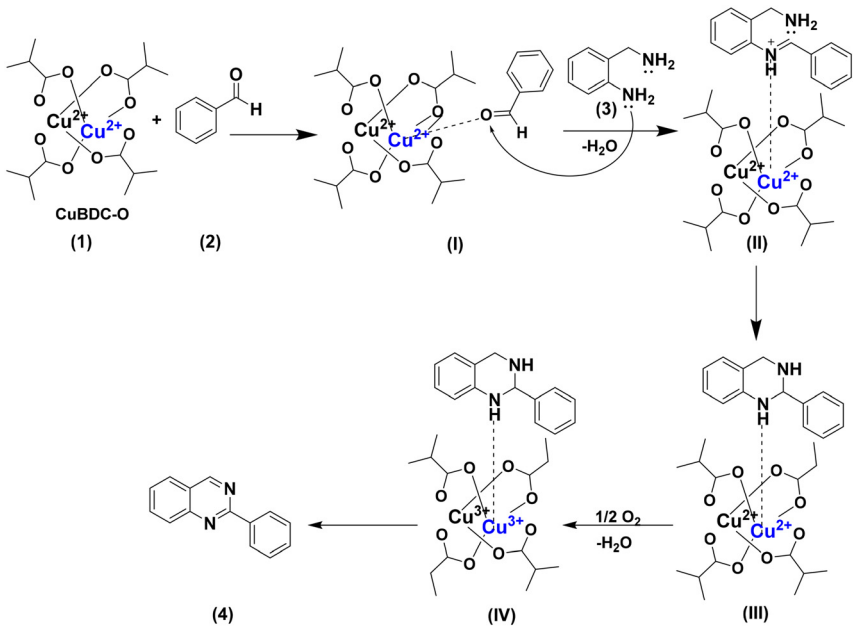

Fig. 7 A proposed mechanism for the synthesis of a quinazoline derivative.

surface area and accessible Cu sites. This performance enhancement demonstrates the functional advantage of morphology-controlled MOF design. It was seen that the catalytic activity of the catalyst persisted for both the reactions even after several cycles, thus proving to be efficient from an economic perspective (Fig. S3, SI).

Conclusion

In conclusion, we were successful in providing an integrated study of morphology, surface area, and particle size-dependent catalytic behavior of CuBDC MOFs, which has not been systematically addressed in prior literature. A clear correlation between the morphology, surface exposure and catalytic activity is established. We have successfully synthesized two CuBDC MOFs with different sizes and morphological attributes just by changing the method of synthesis. Additional CuBDC samples were also prepared to understand the structural effect of the synthesized MOFs. The formation of the CuBDC MOFs was confirmed through collective results of various characterization techniques including XRD, FTIR, XPS, and SEM. It was observed that the change in the morphological property altered the catalytic performance, with CuBDC-O being the potent candidate for the AAC reaction and for the synthesis of 2-substituted quinazolines with excellent yields up to 98% and 99%, respectively. The synthesised CuBDC-O showed good functional group tolerance and was efficient for a wide range of substrates. Therefore, this study uniquely decouples the effects of particle size and morphology on catalytic performance, offering a new understanding of structure–function relationships in MOFs and paving a way for unfolding new horizons in organic scaffolds.

Author contributions

Masshuda Madni Khatun: design, conceptualization, data curation, methodology, formal analysis, and software; Priyanka Gogoi: data curation and methodology; Nilakshi Dutta: data curation and methodology. Puja Pokhrel: methodology. Diganta Sarma: supervision. Kalyanjyoti Deori: conceptualization and supervision.

Conflicts of interest

There is no conflict of interest involved in this work and the authors declare no competing financial interest.

Data availability

The data supporting this article have been included as part of the manuscript.

Supplementary information (SI): SEM elemental mapping, SEM images of CuBDC-P and CuBDC-M, optimization tables, comparison tables, recyclability test, characterization data of 1,2,3-triazole derivatives, ^{1}H NMR and ^{13}C NMR spectra of NH-triazole derivatives, analytical data of 2-substituted quinazolines, and ^{1}H NMR and ^{13}C NMR spectra of 2-substituted quinazolines. See DOI: https://doi.org/10.1039/d5dt02446c.

Acknowledgements

M. M. K is grateful to DST-PURSE for the research fellowship under the DST-PURSE project. P. G. thanks CSIR, New Delhi,

 This journal is © The Royal Society of Chemistry 2025

Published on 05 November 2025. Downloaded on 06.05.26 00:28:10.

for the research fellowship. N. D. expresses gratitude to DST-WISE for fellowship support. We sincerely thank DST-FIST (SR/FST/CS-I/2020/152) and DST-PURSE (SR/PURSE/2022/143 (C)) projects for financial support. We are thankful to Dibrugarh University for providing infrastructural facilities. We acknowledge STIC Cochin for XRD analyses, IIT Roorkee for XPS, IIT Indore for TGA, IASST for BET analysis and Dibrugarh University for NMR and SEM facilities.

References

1 A. Dhakshinamoorthy and H. Garcia, Metal–organic frameworks as solid catalysts for the synthesis of nitrogen-containing heterocycles, *Chem. Soc. Rev.*, 2014, **43**, 5750–5765.
2 E. Niknam, F. Panahi, F. Daneshgar, F. Bahrami and A. Khalafi-Nezhad, Metal–Organic Framework MIL-101(Cr) as an efficient heterogeneous catalyst for clean synthesis of benzoazoles, *ACS Omega*, 2018, **3**, 17135–17144.
3 S. Yadav, S. Sharma, S. Dutta, A. Sharma, A. Adholeya and R. K. Sharma, Harnessing the untapped catalytic potential of a $CoFe_2O_4$/Mn-BDC hybrid MOF composite for obtaining a multitude of 1,4-disubstituted 1,2,3-triazole scaffolds, *Inorg. Chem.*, 2020, **59**, 8334–8344.
4 Y. Yang, K. Guo, Y. Liu, M. Xing, M. Zhu, X. Bai, Y. Lu, Y. Hu and S. Liu, Polyoxometalate-based metal–organic frameworks with both proton acid and multioxidative active sites: highly efficient catalytic synthesis of quinazolinones, *ACS Appl. Mater. Interfaces*, 2024, **16**, 49400–49410.
5 C. Gogoi, N. Nagarjun, S. Roy, S. K. Mostakim, D. Volkmer, A. Dhakshinamoorthy and S. Biswas, Nanomolar level fluorogenic detection of cyanide with an amide Functionalized zirconium metal-organic framework and its application in real-world cyanide monitoring, *Inorg. Chem.*, 2021, **60**, 4539–4550.
6 S. Sk, A. Jamma, D. S. Gavali, V. Bhasin, R. Ghosh, K. Sudarshan, R. Thapa and U. Pal, Modulated ultrathin NiCo-LDH nanosheet-decorated Zr^{3+} rich defective NH_2–UiO-66 nanostructure for efficient photocatalytic hydrogen evolution, *ACS Appl. Mater. Interfaces*, 2023, **15**, 55822–55836.
7 S. Q. Wang, X. Wang, X. M. Cheng, J. Ma and W. Y. Sun, Tailoring defect-type and ligand-vacancies in Zr(IV) frameworks for CO_2 photoreduction, *J. Mater. Chem. A*, 2022, **10**, 16396–16402.
8 K. K. Gangu, S. Maddila, S. B. Mukkamala and S. B. Jonnalagadda, A Review on contemporary metal-organic framework materials, *Inorg. Chim. Acta*, 2016, **446**, 61–74.
9 X. Ma, Y. Chai, P. Li and B. Wang, Metal–organic framework films and their potential applications in environmental pollution control, *Acc. Chem. Res.*, 2019, **52**, 1461–1470.
10 Z. Luo, S. Fan, C. Gu, W. Liu, J. Chen, B. Li and J. Liu, Metal–organic framework (MOF)-based nanomaterials for biomedical applications, *Curr. Med. Chem.*, 2019, **26**, 3341–3369.
11 X. Zhu, H. Zheng, X. Wei, Z. Lin, L. Guo, B. Qiu and G. Chen, Metal–organic framework (MOF): a novel sensing platform for biomolecules, *Chem. Commun.*, 2013, **49**, 1276–1278.
12 F. Gao, X. Tu, X. Ma, Y. Xie, J. Zou, X. Huang, F. Qu, Y. Yu and L. Lu, NiO@Ni-MOF nanoarrays modified Ti mesh as ultrasensitive electrochemical sensing platform for luteolin detection, *Talanta*, 2020, **215**, 120891.
13 A. Herbst, A. Khutia and C. Janiak, Bronsted instead of Lewis acidity in functionalized MIL-101Cr MOFs for efficient heterogeneous (nano-MOF) catalysis in the condensation reaction of aldehydes with alcohols, *Inorg. Chem.*, 2014, **53**, 7319–7333.
14 S. Yadav, R. Dixit, S. Sharma, S. Dutta, K. Solanki and R. K. Sharma, Magnetic metal organic framework composites: structurally advanced catalytic materials for organic transformations, *Mater. Adv.*, 2021, **2**, 2153–2187.
15 C. S. Hinde, W. R. Webb, B. K. Chew, H. R. Tan, W. H. Zhang, T. A. Hor and R. Raja, Utilisation of gold nanoparticles on amine functionalised UiO-66 (NH_2-UiO-66) nanocrystals for selective tandem catalytic reactions, *Chem. Commun.*, 2016, **52**, 6557–6560.
16 J. Yuan, A. M. Fracaroli and W. G. Klemperer, Convergent synthesis of a metal–organic framework supported olefin metathesis catalyst, *Organometallics*, 2016, **35**, 2149–2155.
17 D. T. Genna, A. G. Wong-Foy, A. J. Matzger and M. S. Sanford, Heterogenization of homogeneous catalysts in metal–organic frame works via cation exchange, *J. Am. Chem. Soc.*, 2013, **135**, 10586–10589.
18 M. I. Breeze, G. Clet, B. C. Campo, A. Vimont, M. Daturi, J. M. Greneche, A. J. Dent, F. Millange and R. I. Walton, Isomorphous substitution in a flexible metal–organic framework: mixed-metal, mixed-valent MIL-53 type materials, *Inorg. Chem.*, 2013, **52**, 8171–8182.
19 Y. Y. Liu, K. Leus, T. Bogaerts, K. Hemelsoet, E. Bruneel, V. V. Speybroeck and P. Van Der Voort, Bimetallic–organic framework as a zero-leaching catalyst in the aerobic oxidation of cyclohexene, *ChemCatChem*, 2013, **5**, 3657–3664.
20 P. Wu, X. Guo, L. Cheng, C. He, J. Wang and C. Duan, Photoactive metal–organic framework and its film for light-driven hydrogen production and carbon dioxide reduction, *Inorg. Chem.*, 2016, **55**, 8153–8159.
21 Z. Hu, T. Kundu, Y. Wang, Y. Sun, K. Zeng and D. Zhao, Modulated hydrothermal synthesis of highly stable MOF-808(Hf) for methane storage, *ACS Sustainable Chem. Eng.*, 2020, **8**, 17042–17053.
22 F. N. Azad, M. Ghaedi, K. Dashtian, S. Hajati and V. Pezeshkpour, Ultrasonically assisted hydrothermal synthesis of activated carbon-HKUST-1-MOF hybrid for efficient simultaneous ultrasound-assisted removal of ternary organic dyes and antibacterial investigation: Taguchi optimization, *Ultrason. Sonochem.*, 2016, **31**, 383–393.
23 K. Vo, V. N. Le, D. T. Quang, M. Song, D. Kim and J. Kim, Rapid defect engineering of UiO-67 (Zr) via microwave-assisted continuous-flow synthesis: Effects of modulator

Published on 05 November 2025. Downloaded on 06.05.26 00:28:10.

species and concentration on the toluene adsorption, *Microporous Mesoporous Mater.*, 2020, **306**, 110405.
24 L. H. Wee, S. R. Bajpe and N. Janssens, Convenient synthesis of $Cu_3(BTC)_2$ encapsulated Keggin heteropolyacid nanomaterial for application in catalysis, *Chem. Commun.*, 2010, **46**, 8186–8188.
25 K. Yu, Y. R. Lee, J. Y. Seo, K. Y. Baek, Y. M. Chung and W. S. Ahn, Sonochemical synthesis of Zr-based porphyrinic MOF-525 and MOF-545: Enhancement in catalytic and adsorption properties, *Microporous Mesoporous Mater.*, 2021, **316**, 110985.
26 U. Mueller, M. Schubert, F. Teich, H. Puetter, K. Schierle-Arndt and J. Pastre, Metal–organic frameworks—prospective industrial applications, *J. Mater. Chem.*, 2006, **16**, 626–636.
27 N. Campagnol, T. Van Assche, T. Boudewijns, J. Denayer, K. Binnemans, D. De Vos and J. Fransaer, High pressure, high temperature electrochemical synthesis of metal–organic frameworks: films of MIL-100 (Fe) and HKUST-1 in different, morphologies, *J. Mater. Chem. A*, 2013, **1**, 5827–5830.
28 P. K. Hazarika, P. Gogoi, R. Hazarika, K. Deori and D. Sarma, Nanostructured Ni $(OH)_2$–ZnO mixed crystals as recyclable catalysts for the synthesis of N-unsubstituted 1, 2, 3-triazoles, *Mater. Adv.*, 2022, **3**, 7810–7814.
29 A. Garg, N. Borah, J. Sultana, A. Kulshrestha, A. Kumar and D. Sarma, Silica immobilized copper N-heterocyclic carbene: An effective route to 1,2,3-triazoles via azide-alkyne cycloaddition and multicomponent click reaction, *Appl. Organomet. Chem.*, 2021, **35**, 6298–6308.
30 P. Gogoi, H. Deka, B. Das, K. Deori and D. Sarma, Nanostructured Ag-gCN as a visible light-active copper-free catalyst for azide–alkyne cycloaddition reactions: A sustainable approach to click chemistry, *ACS Sustainable Chem. Eng.*, 2025, **13**, 936–945.
31 P. Gogoi, T. Saikia, R. Hazarika, A. Garg, K. Deori and D. Sarma, Ultralow-loading copper sulfide nanosheets on g-C_3N_4 as a visible-light-active photocatalyst for the regioselective synthesis of 1, 4-disubstituted 1, 2, 3-triazoles, *ACS Sustainable Chem. Eng.*, 2023, **11**, 15207–15217.
32 S. Chetia, S. Sarmah, A. Dutta and D. Sarma, Copper–catalyzed acceptorless dehydrogenative coupling of 2-aminoaryl methanols with nitriles for accessing quinazolines and quinolines, *Eur. J. Org. Chem.*, 2023, e202300390.
33 P. T. K. Arachchige and C. S. Yi, Synthesis of quinazoline and quinazolinone derivatives via ligand-promoted ruthenium-catalyzed dehydrogenative and deaminative coupling reaction of 2-aminophenyl ketones and 2-aminobenzamides with amines, *Org. Lett.*, 2019, **21**(9), 3337–3341.
34 N. Dutta, B. Dutta, A. Dutta, B. Sarma and D. Sarma, Room temperature ligand-free Cu_2O–H_2O_2 catalyzed tandem oxidative synthesis of quinazoline-4 (3 H)-one and quinazoline derivatives, *Org. Biomol. Chem.*, 2023, **21**, 748–753.
35 M. G. Ahmad, M. M. Balamurali and K. Chanda, Click-derived multifunctional metal complexes for diverse applications, *Chem. Soc. Rev.*, 2023, **52**, 5051–5087.
36 B. Li, C. Xu, X. Zhu, J. Yu, X. Zhang and Y. Fan, Green chemistry perspectives on click chemistry approaches for cellulose functionalization: a critical review, *Green Chem.*, 2025, **27**, 6342–6361.
37 V. O. Rodionov, V. V. Fokin and M. Finn, Mechanism of the ligand-free CuI-catalyzed azide-alkyne cycloaddition reaction, *Angew. Chem.*, 2005, **117**, 2250–2255.
38 C. Wang, S. Li, H. Liu, Y. Jiang and H. Fu, Copper-catalyzed synthesis of quinazoline derivatives via ullmann-type coupling and aerobic oxidation, *J. Org. Chem.*, 2010, **75**, 7936–7938.
39 X. Wang, D. He, Y. Huang, Q. Fan, W. Wu and H. Jiang, Copper-catalyzed synthesis of substituted quinazolines from benzonitriles and 2-ethynylanilines via carbon–carbon bond cleavage using molecular oxygen, *J. Org. Chem.*, 2018, **83**, 5458–5466.
40 W. Zhang, X. He, B. Ren, Y. Jiang and Z. Hu, $Cu(OAc)_2{\cdot}H_2O$—An efficient catalyst for huisgen-click reaction in supercritical carbon dioxide, *Tetrahedron Lett.*, 2015, **56**, 2472–2475.
41 R. Murugan, M. B. Reddy, P. Pandurangan and R. Anandhan, Gold-like thiolate-protected ultrasmall cubic copper nanocluster-based metal–organic framework as a selective catalyst for stepwise synthesis of unsymmetric bis-triazole by click reaction, *ACS Appl. Mater. Interfaces*, 2020, **12**, 56004–56016.
42 X. Jia, G. Xu, Z. Du and Y. Fu, Cu (BTC)-MOF catalyzed multicomponent reaction to construct 1, 4-disubstituted-1, 2, 3-triazoles, *Polyhedron*, 2018, **151**, 515–519.
43 S. W. Lee, P. D. Q. Dao, H. J. Lim and C. S. Cho, Recyclable Magnetic Cu-MOF-74-catalyzed C (Sp^2)-N coupling and cyclization under microwave irradiation: synthesis of imidazo [1, 2-c] quinazolines and their analogues, *ACS Omega*, 2023, **8**, 16218–16227.
44 M. Shete, P. Kumar, J. E. Bachman, X. Ma, Z. P. Smith, W. Xu, K. A. Mkhoyan, J. R. Long and M. Tsapatsis, On the direct synthesis of Cu(BDC) MOF nanosheets and their performance in mixed matrix membranes, *J. Membr. Sci.*, 2018, **549**, 312–320.
45 A. Nayak, S. Viegas, H. Dasari and N. Sundarabal, Cu-BDC and Cu_2O derived from Cu-BDC for the removal and oxidation of asphaltenes: a comparative study, *ACS Omega*, 2022, **7**, 34966–34973.
46 A. H. Khoshakhlagh, F. Golbabaei, M. Beygzadeh, F. Carrasco-Marin and S. J. Shahtaheri, Toluene adsorption on porous Cu–BDC@ OAC composite at various operating conditions: optimization by response surface methodology, *RSC Adv.*, 2020, **10**, 35582–35596.
47 C. Wu, X. Chu, X. Wu, H. Zhou, Y. Zeng, D. Wang and W. Liu, Size and morphology control over MOF-74 crystals, *RSC Adv.*, 2024, **14**, 20604–20608.
48 Y. Pan, D. Heryadi, F. Zhou, L. Zhao, G. Lestari, H. Sub and Z. Lai, Tuning the crystal morphology and size of zeolitic imidazolate framework-8 in aqueous solution by surfactants, *CrystEngComm*, 2011, **13**, 6937–6940.
49 N. T. S. Phan, K. K. A. Le and T. D. Phan, MOF-5 as an efficient heterogeneous catalyst for Friedel–Crafts alkylation reactions, *Appl. Catal., A*, 2010, **382**, 246–253.

 This journal is © The Royal Society of Chemistry 2025

Published on 05 November 2025. Downloaded on 06.05.26 00:28:10.

50 X. Zhang, Y. Xu and B. Ye, An efficient electrochemical glucose sensor based on porous nickel-based metal organic framework/carbon nanotubes composite (Ni-MOF/CNTs, *J. Alloys Compd.*, 2018, **767**, 651–656.
51 G. Gumilar, S. Chatterjee, Y. V. Kaneti, J. Na, J. Henzie, B. Yuliarto, N. Nugraha, A. Patah, A. Bhaumik and Y. Yamauchi, General synthesis of hierarchical sheet/plate-like M-BDC (M = Cu, Mn, Ni, and Zr) metal–organic frameworks for electrochemical non-enzymatic glucose sensing, *Chem. Sci.*, 2020, **11**, 3644–3655.
52 K. Huang, Y. Xu, L. Wang and D. Wu, Heterogeneous catalytic wet peroxide oxidation of simulated phenol wastewater by copper metal–organic frameworks, *RSC Adv.*, 2015, **5**, 32795–32803.
53 T. Q. Tran, H. M. Tran, X. T. Nguyen, D. T. Nguyen, P. L. T. Giang and N. T. Nguyen, Fabrication of copper-terephthalate frameworks and N-doped carbon dots composite for boosting photocatalytic performance, *Top. Catal.*, 2023, **66**, 104–116.
54 S. Adhikari, D. Sarkar and G. Madras, Hierarchical design of CuS architectures for visible light photocatalysis of 4-Chlorophenol, *ACS Omega*, 2017, **2**, 4009–4021.
55 A. Taher, D. W. Kim and I. Lee, Highly efficient metal organic framework (MOF)-based copper catalysts for the base-free aerobic oxidation of various alcohols, *RSC Adv.*, 2017, **7**, 17806–17812.
56 N. A. Surib, A. Kuila, P. Saravanan, L. C. Sim and K. H. Leong, A ligand strategic approach with Cu-MOF for enhanced solar light Paper a ligand strategic approach with Cu-MOF for enhanced solar light photocatalysis, *New J. Chem.*, 2018, **42**, 11124–11130.
57 M. Rong, L. Lin, X. Song, T. Zhao, Y. Zhong, J. Yan, Y. Wang and X. Chen, A label-free fluorescence sensing approach for selective and sensitive detection of 2,4,6-Trinitrophenol (TNP) in aqueous solution using graphitic carbon nitride Nanosheets, *Anal. Chem.*, 2015, **87**, 1288–1296.
58 J. Qin, S. Wang, H. Ren, Y. Hou and X. Wang, Photocatalytic reduction of CO_2 by graphitic carbon nitride polymers derived from urea and barbituric acid, *Appl. Catal., B*, 2015, **179**, 1–8.
59 D. N. G. Krishna and J. Philip, Review on surface-characterization applications of X-ray photoelectron spectroscopy (XPS): Recent developments and challenges, *Appl. Surf. Sci.*, 2022, **12**, 100332.
60 J. Wang, I. Imaz and D. Maspoch, Metal–organic frameworks: why make them small?, *Small Struct.*, 2022, **3**, 2100126.
61 R. Hazarika, S. Dutta, S. Sarmah, P. K. Hazarika, K. Singh, A. Kumar, B. Sarma and D. Sarma, PCy_3-assisted Ag(I) Catalysed Click Reaction for Regioselective Synthesis of 1, 4-disubstituted 1, 2, 3 triazoles at Room Temperature, *Org. Biomol. Chem.*, 2024, **22**, 694–698.
62 H. B. E. L. Ayouchia, L. Bahsis, H. Anane, L. R. Domingo and S. E. Stiriba, Understanding the mechanism and regioselectivity of the copper(I) catalyzed [3 + 2] cycloaddition reaction between azide and alkyne: A systematic DFT study, *RSC Adv.*, 2018, **8**, 7670–7678.
63 L. Liang and D. Astruc, The copper(I)-catalyzed alkyne-azide cycloaddition (CuAAC) "click" reaction and its applications. An overview, *Coord. Chem. Rev.*, 2011, **255**, 2933–2945.
64 G. Latha, N. Devarajan and P. Suresh, Framework copper catalyzed oxidative synthesis of quinazolinones: a benign approach using $Cu_3(BTC)_2$ MOF as an efficient and reusable catalyst, *ChemistrySelect*, 2020, **5**, 10041–10047.